

SAR Imaging of Waves in Water and Ice: Evidence for Velocity Bunching

D. R. LYZENGA, R. A. SHUCHMAN, AND J. D. LYDEN

Radar Division, Environmental Research Institute of Michigan, Ann Arbor

C. L. RUFENACH

Wave Propagation Laboratory, NOAA Environmental Research Laboratory, Boulder, Colorado

Synthetic aperture radar (SAR) images collected over the Arctic marginal ice zone show gravity wave patterns in both the open water and the ice. Diffuse wave patterns are visible in the water at near range (small incidence angles), while more distinct wave patterns are visible in the ice across the entire swath. The wave patterns in the ice appear as bright lines rather than sinusoidal intensity variations. Additionally, the images show a periodic displacement of the ice/water boundary, apparently due to Doppler shift effects associated with the gravity wave orbital motions. These observations are interpreted as evidence for the velocity bunching effect and also illustrate the effects of random scatterer motions in the open water.

1. INTRODUCTION

Imaging of gravity waves in the ocean by synthetic aperture radar (SAR) has been amply demonstrated by several investigators [Gonzalez *et al.*, 1979; McLeish *et al.*, 1980; Shuchman *et al.*, 1983], although there is still disagreement as to the exact mechanisms responsible for this imaging. In particular, the relative importance of hydrodynamic modulation, tilt modulation, and velocity bunching is not well known [Alpers *et al.*, 1981; Harger, 1981; Jain, 1981]. Additionally, there remains some controversy regarding the effects of random scatterer velocities and accelerations on the spatial resolution of the SAR imagery [Raney, 1981; Beal *et al.*, 1983; Lyzenga and Shuchman, 1983].

SAR imaging of waves in ice has also been previously reported [Raney and Lowry, 1978; Dawe and Parashar, 1978; Lyden *et al.*, 1982] and the modulation mechanisms for such imaging have been qualitatively discussed. This paper presents imagery of waves in both open water and ice, along with calculations which suggest that velocity bunching is the dominant modulation mechanism for these waves. The effects of random scatterer motions on the water surface are also illustrated, and their implications for the wave imaging process are discussed.

2. DATA DESCRIPTION

The SAR data discussed in this paper were collected over the Arctic marginal ice zone using the X-L SAR system, which is jointly owned by the Canada Centre for Remote Sensing and the Environmental Research Institute of Michigan (ERIM) [Lyden *et al.*, 1982]. The relevant system parameters for this data set are given in Table 1. Two portions of the X band imagery from a single pass, separated by about 20 km in the along-track direction, are shown in Figures 1 and 2. The image shown in Figure 1 is over open water, while the area shown in Figure 2 is partially covered by a layer of fragmented ice.

A wave pattern can be seen faintly in the open water

(Figure 1) at near range, and quite clearly in the ice (Figure 2) across the entire swath, propagating from the upper right to the lower left side of each image. The intensity variations in the ice are distinctly nonsinusoidal and appear as bright, narrow lines. The intensity variations in the water are more diffuse and more nearly sinusoidal in appearance. Also visible in the water image are bright streaks aligned in the along-track direction, which are similar to the phenomena discussed by Lyzenga and Shuchman [1983].

Representative intensity profiles through the wave patterns in the ice and in the water are shown in Figures 3 and 4. These measurements were made in the ERIM optical processor. Although the signal levels indicate that the radar was operating in the linear region of its response curve, it is interesting to note that even when radar saturation occurs, the local image contrast is preserved in the processed SAR image [Livingstone *et al.*, 1984]. Therefore these plots are felt to be accurate representations of the true image intensity and are not distorted by any system effects peculiar to this data set. Two-dimensional spectra of the image intensity, generated from digitizations of the image intensity in the optical processor, are shown in Figures 5 and 6. The open water spectrum (Figure 5) shows a line along the range wave number axis which is due to the image streaks mentioned above. The nonsinusoidal nature of the intensity variations in the ice is manifested in the harmonics visible in Figure 6. The dominant wavelength is approximately 120 m, and the direction is approximately 45° from the range direction. A possible secondary wave component also appears in Figure 6 in roughly an orthogonal direction.

Another important feature of this data is indicated by the arrows in Figure 2. The ice edges in this image are periodically displaced in the along-track direction with a periodicity equal to that of the wave pattern. These displacements are apparently due to the Doppler shift effect described by Raney [1971] and are directly related to the velocity bunching mechanism discussed by Alpers *et al.* [1981]. A further analysis of this phenomenon is given in the following section.

3. DISCUSSION

Although there is very little "surface truth" information available for this data set, some inferences can be made about

TABLE 1. CCRS/ERIM X Band SAR System and Processing Parameters

Parameter	Value
Radar Wavelength, λ	3.2 cm
Platform Velocity, V	125 m/s
Platform Altitude, A	2.5 km
Antenna Beamwidth, β	1.1°
Azimuth Bandwidth, B	40 Hz
Processed Resolution, ρ_0	3 m

$$\Delta X = \frac{R}{V} V_r \tag{1}$$

where V_r is the radial velocity of the surface, R is the range distance, and V is the platform velocity. The surface elements moving away from the SAR are displaced in the opposite direction. A maximum along-track displacement of about ± 30 m is observed for the edges shown in Figure 5, which are at a range of approximately 7.5 km. The radial velocity necessary to cause this displacement is

$$(V_r)_{\max} = \frac{V}{R} \Delta X = \pm 0.5 \text{ m/s} \tag{2}$$

the relative importance of various imaging mechanisms based upon the SAR data itself. First, it is possible to estimate the wave height by measuring the displacement of the ice edge shown in Figure 2. The surface elements moving toward the SAR (due to the wave orbital motion) are displaced in the along-track direction (i.e., to the right) by an amount

where $V = 125$ m/s is the platform velocity. For a sinusoidal wave of length L and crest-to-trough height H , traveling at an angle ϕ with respect to the along-track direction, the maximum radial velocity due to the orbital motion of the wave

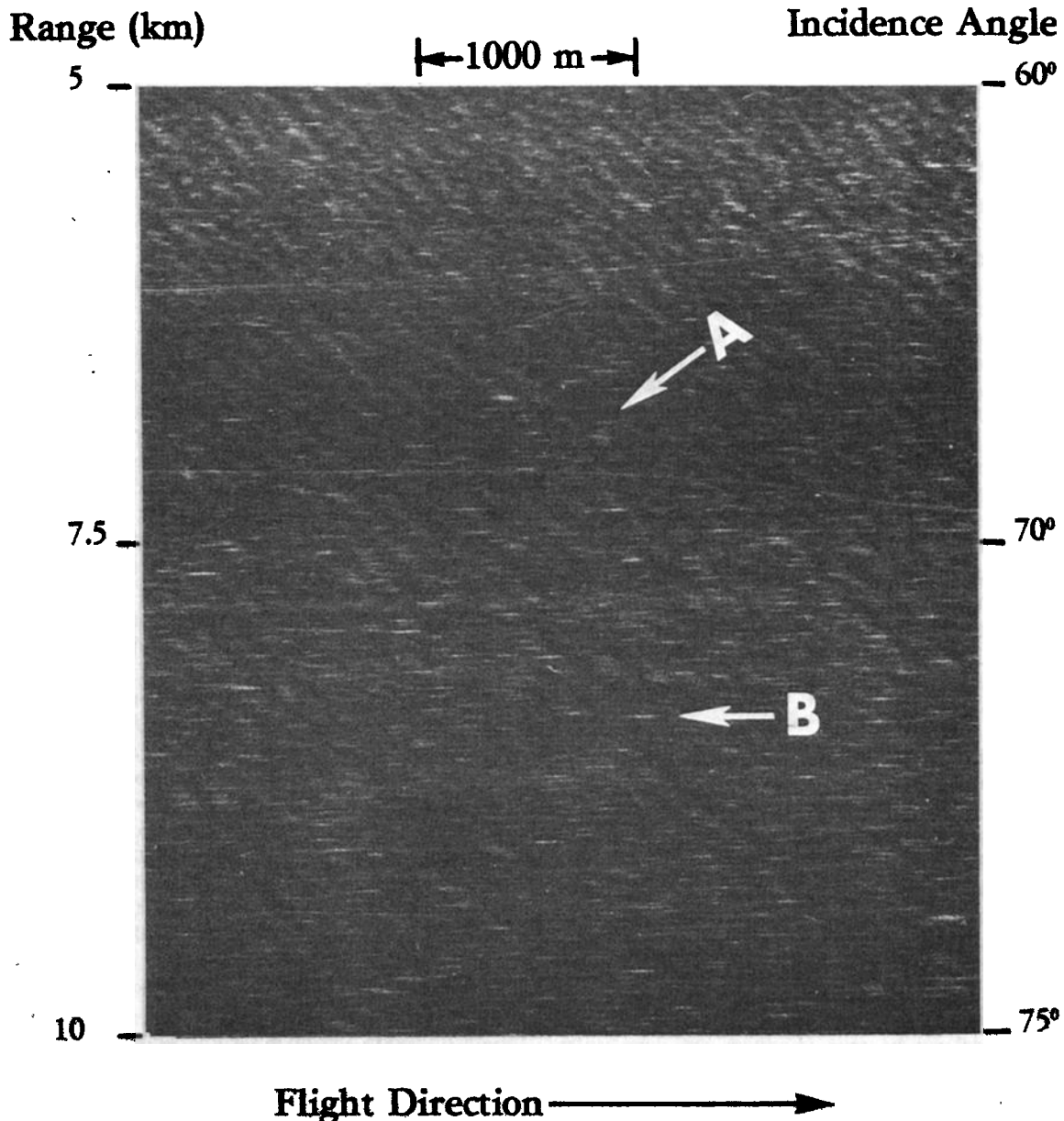


Fig. 1. X band SAR image over open water approximately 10 km outside ice edge. Arrow A indicates direction of wave propagation and B indicates azimuth streaks discussed in text.

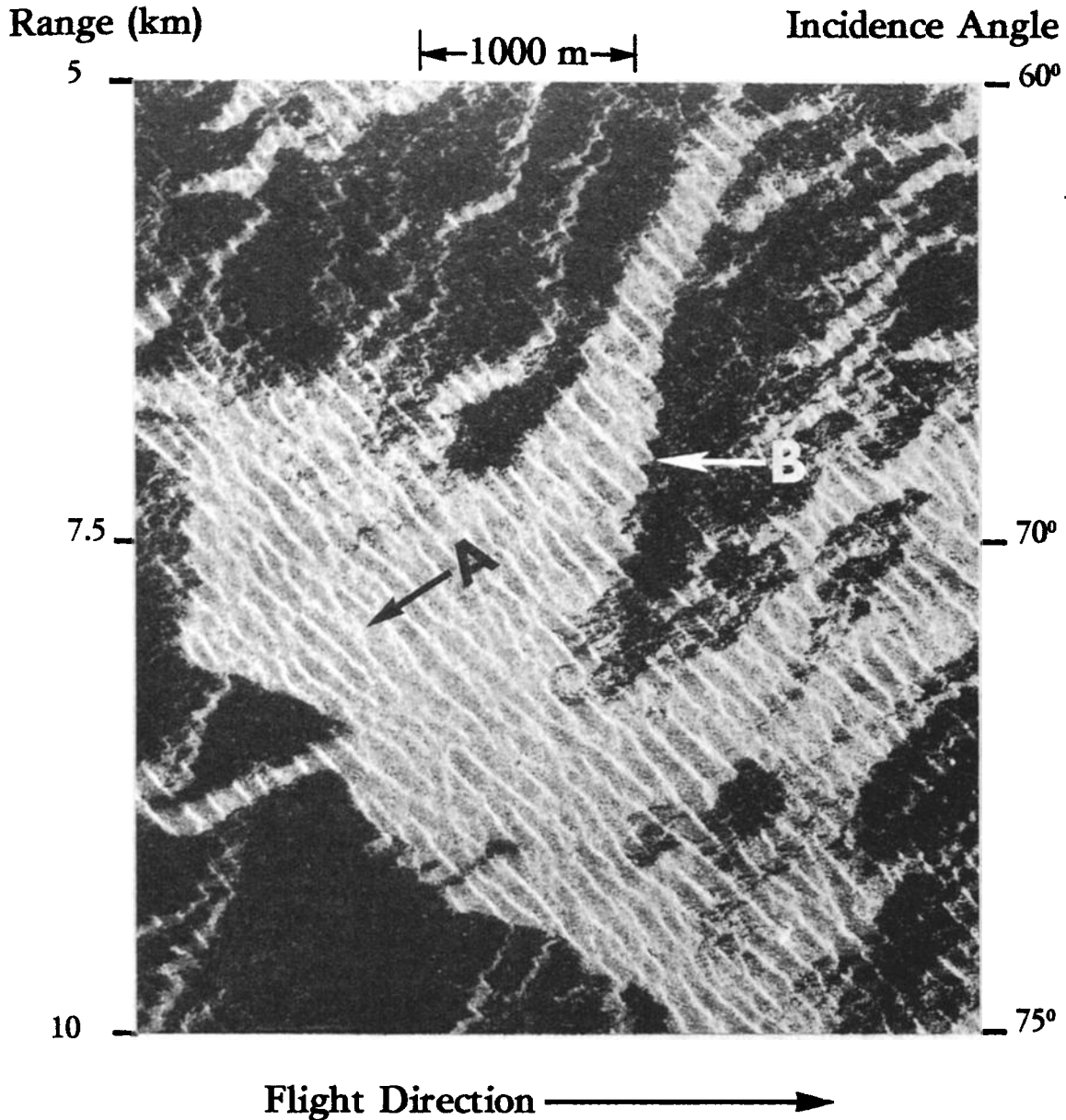


Fig. 2. X band SAR image showing waves in ice (A) and periodic displacement of ice edge (B). Location of this image is approximately 20 km from Figure 1.

(observed at an incidence angle θ) is

$$(V_r)_{\max} = \frac{H}{2} \omega f(\theta, \phi) \quad (3)$$

where $k = 2\pi/L$, $\omega = \sqrt{gk}$, and

$$f(\theta, \phi) = (\sin^2 \theta \sin^2 \phi + \cos^2 \theta)^{1/2} \quad (4)$$

[Alpers et al., 1981]. Thus the observed displacement of the ice edge implies a crest-to-trough height of

$$H = \frac{2(V_r)_{\max}}{\omega f(\theta, \phi)} = 1.8 \text{ m} \quad (5)$$

based on an observed wavelength L of 120 m, a wave direction ϕ of 45° , and an incidence angle θ of 70° .

The observed displacement of scatterers at the ice edge also

implies a periodic increase and decrease in the image intensity within a homogeneous area of ice or water, which is referred to as the velocity bunching effect [Alpers et al., 1981]. An expression for the magnitude of this effect is given by

$$I(x, y) = \iint \sigma_0(x', y') \frac{1}{\rho_x \rho_y} \cdot \exp \left\{ -\frac{\pi}{\rho_x^2} \left[x - x' - \frac{R}{V} V_r(x', y') \right]^2 - \frac{\pi}{\rho_y^2} [y - y']^2 \right\} dx' dy' \quad (6)$$

where $\sigma_0(x', y')$ is the radar cross section per unit area of the surface, $V_r(x', y')$ is the radial component of the orbital velocity of the wave, ρ_x is the azimuth resolution (including the effects

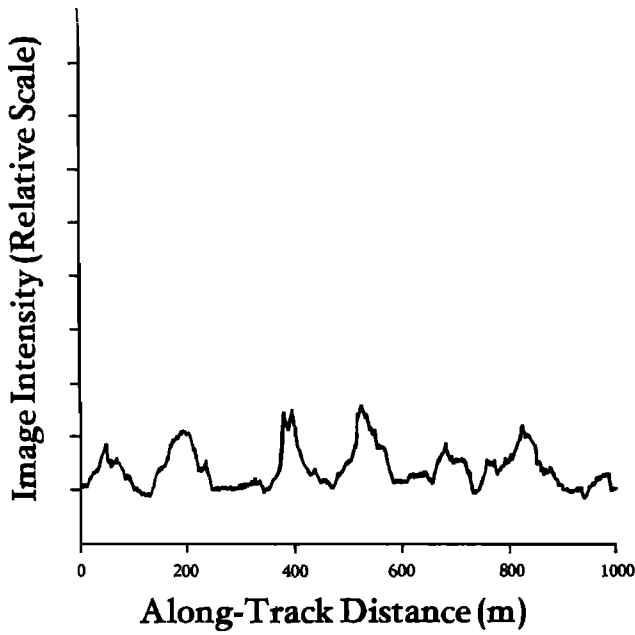


Fig. 3. Image intensity profile through waves in open water at a range of 5 km.

of orbital accelerations and random scatterer motions), and ρ_y is the range resolution of the system. This expression was evaluated using the wave parameters discussed above, assuming a uniform surface radar cross section and an azimuth resolution

$$\rho_x = \left[(\rho_0)^2 + \left(\frac{\beta R^2 a_r}{V^2} \right)^2 \right]^{1/2} \quad (7)$$

where a_r is the radial acceleration due to the wave orbital motion, and the other parameters are as defined in Table 1.

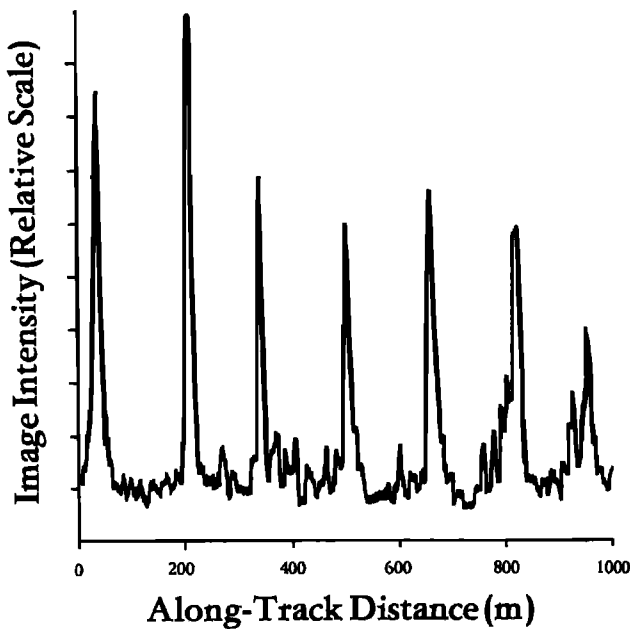


Fig. 4. Image intensity profile through waves in ice at a range of 10 km.

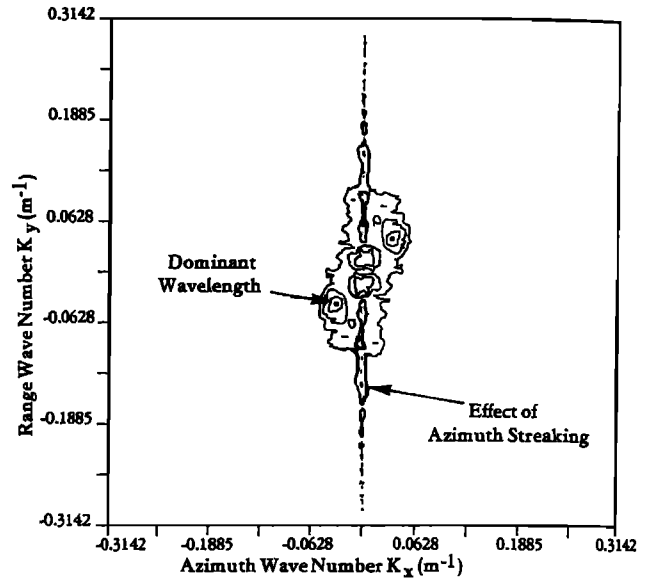


Fig. 5. Two-dimensional spectrum of image intensity over waves in open water. Plot shows logarithm of spectral density with 3-dB contour intervals.

The calculation also included the effects of the system azimuth bandwidth by excluding the contributions from scatterers moving at radial velocities greater than

$$V_m = \lambda B/4 \quad (8)$$

where B is the azimuth bandwidth of the SAR system, including the processor. This bandwidth limiting eliminates the effects of any scatterers moving at the phase velocity of the gravity wave, since such scatterers would fall outside the azimuth passband.

A one-track plot of the results of this simulation in the along-track direction is shown in Figure 7 for two values of the range distance or incidence angle. The results are only

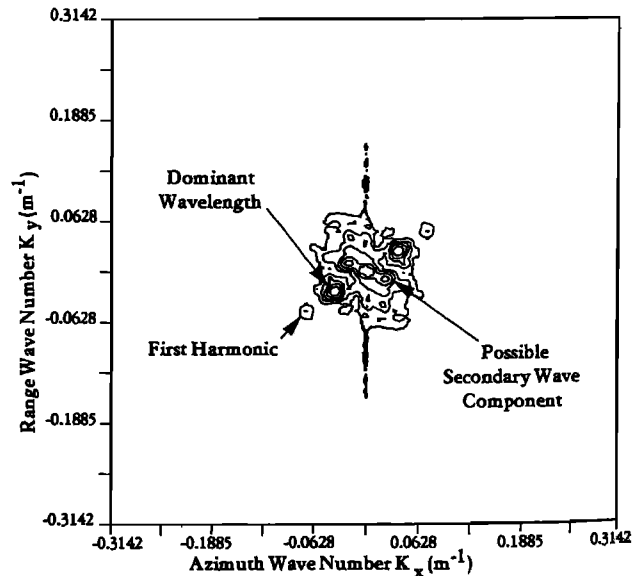


Fig. 6. Two-dimensional spectrum of image intensity over waves in ice. Plot shows logarithm of spectral density with 3-dB contour intervals.

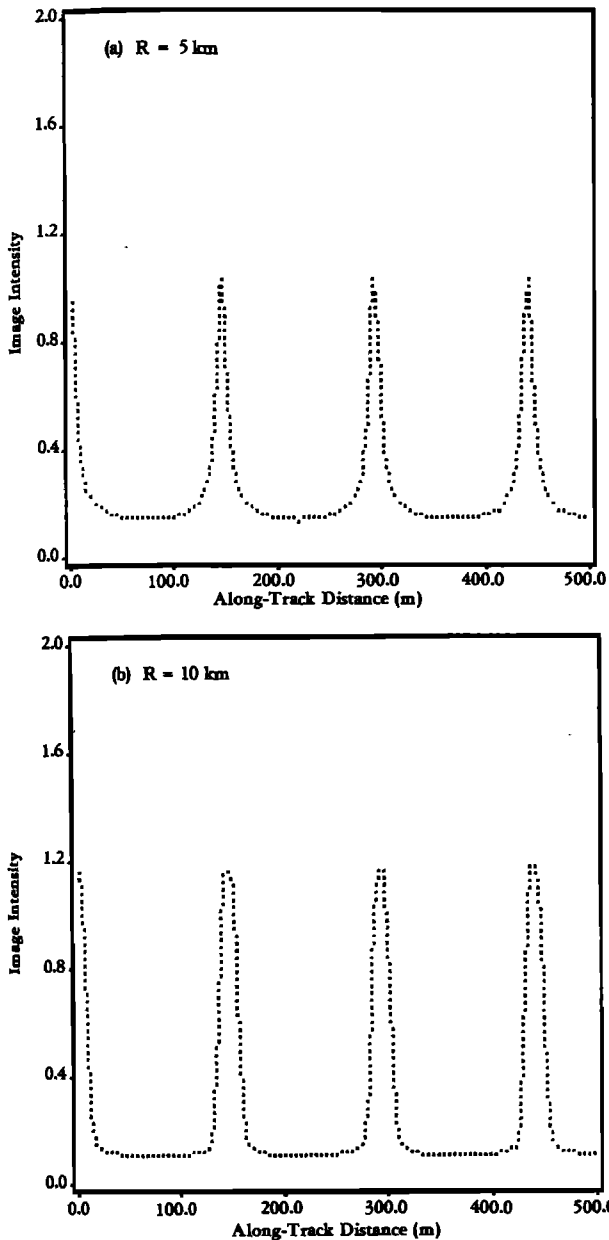


Fig. 7. Calculated image intensity variations over waves in ice at $R = 5$ km and $R = 10$ km.

weakly dependent on the incidence angle, so that a uniform wave image is predicted across the swath. Note the strongly nonsinusoidal form of the intensity profile, which agrees quite well with the observed intensity distribution for the waves in the ice.

A possible explanation of the lower contrast as well as the more nearly sinusoidal intensity of the waves in the water (Figure 3) is the effect of random scatterer motions due to shorter waves in the water, which are not present in the ice. The effect of these random motions may be described in terms of the coherence time of the microwave return [Raney, 1981]. This finite coherence time causes a degradation in the azimuth resolution, which is dependent on the range distance as expressed by the equation

$$\rho_x = \left[(\rho_0)^2 + \left(\frac{\beta R^2 a_r}{V^2} \right)^2 + \left(\frac{\lambda R}{2V\tau} \right)^2 \right]^{1/2} \quad (9)$$

where τ is the coherence time, and the other parameters are the same as in (7). Note that the streaks in Figure 1 may be interpreted as point scatterers which are imaged with a reduced azimuthal resolution as given by (9) with $\tau \sim 10^{-2}$ s. This value is also consistent with previous X band observations [Lyzena and Shuchman, 1983]. The simulations shown in Figure 7 were repeated with a value of $\tau = 0.01$ s, resulting in the image intensities plotted in Figure 8. The shape of the intensity profile, as well as the degree of modulation shown in Figure 8a is similar to that plotted in Figure 3, which was measured at $R = 5$ km. At a range of 10 km, no waves are visible in the water, as predicted by the very weak modulation shown in Figure 8b.

4. CONCLUSIONS

A velocity bunching model appears to explain the shape and intensity of the wave modulations appearing in both open

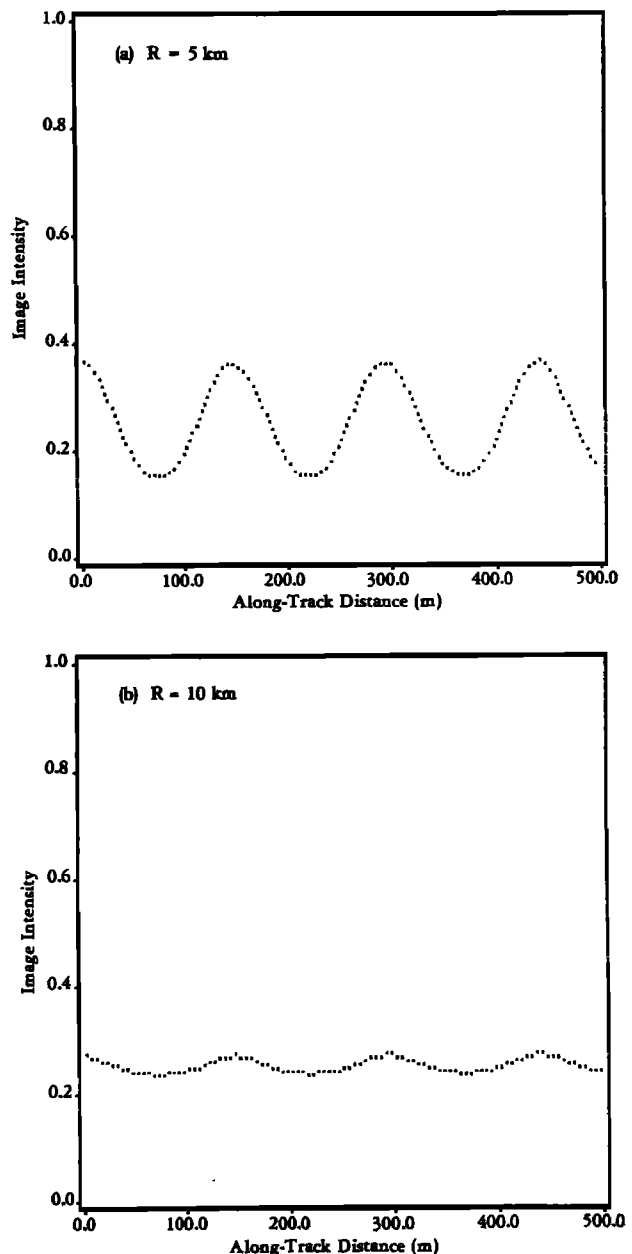


Fig. 8. Calculated image intensity variations over waves in open water at $R = 5$ km and $R = 10$ km.

water and ice-covered water in the images examined in this paper. The image displacements responsible for this modulation are directly observable at the ice edges. The difference between the wave modulations in open water and ice appear to be due to the effects of random scatterer motions or the finite coherence time of the scattered microwave return from the water surface. A coherence time on the order of 10^{-2} s appears to yield the observed wave modulations in the water, which is consistent with previous observations.

Acknowledgments. This research was sponsored by NASA and ONR under contract N00014-81-C-0692. The NASA technical monitor was Lawrence McGoldrick and the ONR technical monitor was Hans Dolezalek. We would like to thank Alex Klooster of ERIM for optically processing the data and making the image intensity measurements presented in this paper.

REFERENCES

- Alpers, W. R., D. B. Ross, and C. L. Rufenach, On the detectability of ocean surface waves by real and synthetic aperture radar, *J. Geophys. Res.*, **86**, 6481-6498, 1981.
- Beal, R. C., D. G. Tilley, and F. M. Monaldo, Large- and small-scale spatial evolution of digitally processed ocean wave spectra from SEASAT synthetic aperture radar, *J. Geophys. Res.*, **88**, 1761-1778, 1983.
- Dawe, B. R., and S. K. Parashar, SAR Imaging of Waves in Ice, *Oceans '78*, IEEE/MTS, 379-384, 1978.
- Gonzalez, F. I., R. C. Beal, W. E. Brown, P. S. DeLeonibus, J. W. Sherman, J. F. R. Gower, D. Lichy, D. B. Ross, C. L. Rufenach, and R. A. Shuchman, Seasat synthetic aperture radar: Ocean wave detection capabilities, *Science*, **204**, 1418-1421, 1979.
- Harger, R. O., SAR ocean imaging mechanisms, in *Spaceborne Synthetic Aperture Radar for Oceanography*, edited by R. C. Beal, P. S. DeLeonibus, and I. Katz, Johns Hopkins University Press, Baltimore, 1981.
- Jain, A., SAR imaging of ocean waves: Theory, *IEEE J. Oceanic Eng.*, **OE-6**, 130-139, 1981.
- Livingstone, C. E., D. Hudson, J. D. Lyden, C. L. Liskow, R. A. Shuchman, and R. T. Lowry, Gain compression in synthetic aperture radar imagery: Theoretical and experimental evidence, *IEEE Trans. Geosci. Remote Sensing*, in press, 1984.
- Lyden, J. D., B. A. Burns, R. A. Shuchman, D. R. Lyzenga, R. W. Larson, and R. T. Lowry, Synthetic aperture radar imagery of ocean waves in sea ice processes, paper presented at International Symposium on Remote Sensing of Environment, Second Thematic Conference on Remote Sensing for Exploration Geology, Environ. Res. Inst. Mich., Fort Worth, Texas, December 6-10, 1982.
- Lyzenga, D. R., and R. A. Shuchman, Analysis of scatterer motion effects in MARSEN X band SAR imagery, *J. Geophys. Res.*, **88**, 9769-9775, 1983.
- McLeish, W., D. B. Ross, R. A. Shuchman, P. G. Teleki, S. V. Hsiao, O. M. Shemdin, and W. E. Brown, Synthetic aperture radar imaging of ocean waves: Comparison with wave measurements, *J. Geophys. Res.*, **85**, 5003-5011, 1980.
- Raney, R. K., Synthetic aperture imaging radar and moving targets, *IEEE Trans. Aerospace Elect. Syst.*, **AES-7**, 499-505, 1971.
- Raney, R. K., Wave orbital velocity, fade and SAR response to azimuth waves, *IEEE J. Oceanic Eng.*, **OE-6**, 140-146, 1981.
- Raney, R. K., and R. T. Lowry, Oceanic wave imagery and wave spectra distortions by synthetic aperture radar, paper presented at 12th International Symposium on Remote Sensing of Environment, Environ. Res. Inst. Mich., Manila, Philippines, April 1978.
- Shuchman, R. A., W. Rosenthal, J. D. Lyden, D. R. Lyzenga, E. S. Kasischke, H. Gunther, and H. Linne, Analysis of MARSEN X Band SAR ocean wave data, *J. Geophys. Res.*, **88**, 9757-9768, 1983.
- D. R. Lyzenga, R. A. Shuchman, and J. D. Lyden, Radar Division, Environmental Research Institute of Michigan, Ann Arbor, MI 48107.
- C. L. Rufenach, Wave Propagation Laboratory, NOAA Environmental Research Laboratory, Boulder, CO 80803.

(Received July 27, 1983;
accepted August 17, 1984.)